10.5 MOUNTAIN WAVES ENTERING THE STRATOSPHERE: NEW AIRCRAFT DATA ANALYSIS TECHNIQUES FROM T-REX

Ronald B. Smith[1], Bryan K. Woods[1], Jorgen Jensen[2], William A. Cooper[2], James D. Doyle[3], Qingfang Jiang[4], Vanda Grubišić[5]

[1]Yale University, New Haven, CT
[2]NCAR/UCAR, Boulder, CO
[3]Naval Research Laboratory, Monterey, CA
[4]UCAR, Monterey, CA
[5]Desert Research Institute, Reno, NV

1. FLIGHT TRACK DESIGN

During the T-Rex project in March and April 2006, the new NSF/NCAR Gulfstream V (GV) research aircraft (Fig. 1) made twelve flights over the Sierra Nevada Range in California to observe mountain waves propagating from the troposphere into the stratosphere (Table 1). To make these flights as useful as possible, a similar wind-oriented racetrack pattern (Fig. 2) was flown during each event, cutting across two similar sections of the Sierra terrain. Altitudes of 9, 11, 13km were emphasized as they spanned the tropopause on most events (Fig. 3). Systematic patterns and altitude changes were possible within a military control area over the Sierras. Typically, flight missions were scheduled to coincide with the passage of baroclinic troughs bringing brief episodes of strong cross-barrier wind (Fig. 4).

In this preliminary report, we limit our discussion to six flights during which the wind direction was near 245 True: our so-called Track B direction. We computed statistics from 126 legs, including the north and south legs for each racetrack for each flight. As seen in Table 1, each flight shows considerable variability in the amplitude of vertical wind velocity and temperature fluctuations. In general, flights RF 4, 5, and 10 found strong waves while RF 6, 8 and 9 found weak waves. While it may be just coincidence, the three strong wave events corresponded to the three strongest cross-mountain ridge-top winds, as determined by averaging 700hPa data from upstream balloon soundings (i.e. Lamoore and Visalia). The data suggests a sharp threshold of 15m/s for large wave generation.

The wind and stability profiles were similar for the six flights. Each wind profile had strong positive unidirectional wind shear in the troposphere with a maximum wind speed of U ~ 45m/s at the tropopause near 10km. Aloft near Z = 21km, the wind weakened to less than 10m/s or to zero in some cases. The temperature profiles showed some static stability just above mountain top from 3 to 4 km, weaker stability in the upper troposphere, and much stronger stability in the stratosphere. The frequent critical level at 21km over the Sierras prevents it from being a major source of gravity waves for the upper stratosphere and mesosphere (Jiang et al, 2002).

Corresponding author address: Ronald B. Smith, Yale University. P.O. 208109, New Haven, CT 06520-8109. E-mail: Ronald.Smith@yale.edu

2. SAMPLE FLIGHT LEVEL DATA

To gain a sense of the data, we present in Figure 5 a set of vertical velocity plots for racetracks at three elevations. For reference, the underlying terrain is presented in Figure 3. The distance coordinate is aligned with Track B and centered at Independence, CA in the Owens Valley.

Data from the north and south legs are shown. The two waves are not perfectly periodic, nor do they line up perfectly between the parallel legs. While some small waves are seen upwind of the Sierra crest, all the large waves are downstream, supporting the idea that the waves are generated by the Sierras. In the sections that follow, we analyze the statistical properties of these waves to reveal their physical nature and to pose salient questions for modelers and theoreticians. The current results are based on an un-validated preliminary data set.

3. WAVE ENERGY DENSITY

One important quantity in the diagnosis of gravity waves is the energy density (Gill, 1982). In trapped waves, the volume integrated kinetic and potential energies are equal (i.e. KE = PE); so-called "energy equipartition". In simple vertically propagating waves, the area integrated KE = PE at each level in the atmosphere. The ratio of vertical to horizontal KE can sometimes be interpreted in terms of the degree of hydrostatic balance.

In the present situation, we integrate the energy contributions over the 180km-long flight legs, defined as our coordinate x_B, giving energy densities with units J/m2. The means are removed from all primed quantities. The horizontal kinetic energy is

$$KE_H = (\overline{\rho}/2)\int (u'^2 + v'^2)\,dx_B \qquad (1)$$

The vertical kinetic energy is

$$KE_Z = (\overline{\rho}/2)\int w'^2 dx_B \quad (2)$$

The potential energy is a measure of the lifting of cold heavy air and depression of warm light air. If the background stability frequency is not known, we use

$$PE = -(\overline{\rho}g/2T)\int \theta'\eta' dx_B \quad (3)$$

If N^2 is known, from the aircraft data itself or nearby balloon data, we can use

$$PE = (\overline{\rho}/2)N^2\int \eta'^2 dx_B \quad (4)$$

The vertical parcel displacement in (3, 4) can be computed in the present case from

$$\eta(s) = \int_0^s \frac{w(s)}{U(s)}ds + \eta(0) \quad (5)$$

if the flow is steady and the aircraft track is parallel to the wind direction. We confirmed that (3) and (4) give similar answers when N^2 in (4) is evaluated from the upstream soundings.

As shown in Table 1, there is general agreement with the equipartition principle. This is especially true in the stratosphere where a linear regression between KE and PE yields a slope near unity. In the upper troposphere on the other hand, the KE exceeds the PE by a factor of five or so. As shown in Figure 6, the PE is small at 9km and 10km but large in the stratosphere (i.e. above 10km) where large wave-induced temperature fluctuations arise from vertically displacing air parcels in a region with a large potential temperature lapse rate. As the temperature perturbations rise in the stratosphere, so to do the horizontal velocity perturbations. In the kinetic energy, the vertical motion makes a rather small contribution compared to the horizontal motions, an indication that the parcel motions are gently sloping.

4. MOMENTUM AND ENERGY FLUX

An essential property of mountain waves is their flux of momentum and energy. We define these quantities by

$$MF_{xB} = \overline{\rho}\int u_B' w' dx_B \quad (6)$$

$$EF = \int p' w' dx_B \quad (7)$$

According to Eliassen and Palm (1961), in steady non-dissipative flow, the two fluxes are related by

$$EF = -U * MF \quad (8)$$

where U is the mean flow speed. While the momentum flux (6) has frequently been computed from aircraft data, the energy flux (7) has never been directly computed from data. The availability of GPS altitude data makes the computation of EF possible for the first time. As the aircraft altitude varies as it flies through the wave, we must correct the measured static pressure to a common level using

$$p_{CORR} = p + \overline{\rho}g(z - z_{REF}) \quad (9)$$

In practice, as the aircraft nearly flies on a constant pressure surface, the first term in (9) makes the smaller contribution. The second term, derived from the GPS altitude data, is dominant in the calculation of (7). As shown in Figure 7, there is a nice linear relationship between MF and EF. A linear regression gives a slope of about 38m/s that is approximately the same as the average flight level wind speed for the three large wave events; about 40 m/s, as predicted by (8). The scatter in Figure 7 might be reduced if the variation in flight level wind speed was accounted for, the pressure calibration was improved and a differential correction was applied to the GPS altitude data.

The reader will notice in Figure 7 that there are some large negative EF values and corresponding positive MF values. Such values would not be found in simple vertically propagating or trapped mountain waves. Further inspection shows that in strong wave flights 4 and 5, all the MF values are negative and all the EF values are positive; consistent with vertically propagating waves (Fig. 8). In flight 10 however, the EF is positive below 12km and negative above 12km. This curious profile of EF and MF presents a challenge to wave theorists and modelers. It suggests that wave energy is converging on the 12km level from below and above.

5. SPECTRA AND PHASE RELATIONSHIPS FOR DOMINANT WAVES

A further analysis of mountain waves can be accomplished with spectral decomposition. To do this we interpolate the one-second flight level data onto a 200 meter grid, remove the mean, taper the ends of the record and apply a Fast Fourier Transform. The spectral peak is considered to be the dominant wavenumber. In (Table 1) we see that the dominant wavelength varies from case to case, but 15 km is most common. The large waves in RF4 and RF10 are systematically longer (30 to 40km), but RF10 has some shorter waves at high altitudes.

The phase relationships between the different wave variables can clarify several aspects of the wave dynamics. As a first step, we examine the phase of the potential temperature and vertical velocity. We assume that the background $\Theta(z)$, is a function of altitude only, and that

$\frac{D\theta}{Dt} = \theta_t + U\theta_x + w'\Theta_z = 0$. If a wave of vertical velocity $w' \sim \hat{w}e^{i(\sigma t + kx)}$ distorts the theta field then

$$\hat{\theta} = \frac{\hat{w}\Theta_z}{(i\sigma + ikU)} = \frac{-i\hat{w}\Theta_z}{\sigma + kU} \qquad (10)$$

According to (10), if the wave is not growing or decaying (i.e. $IM(\sigma) = 0$), U>0 and $\Theta_z > 0$ then theta lags w by 90 degrees. In Figure 9a showing the co- and quad-spectrum for w and theta for each leg, the points cluster about a 90 degree phase shift, thus supporting the above assumptions. If the wave is steady, the ratio of theta and w magnitudes is Θ_z / kU.

A more useful analysis examines the three-way balance expressed in the steady linearized horizontal momentum equation

$$Uu'_x + U_z w' = (-1/\rho)p_x \qquad (11)$$

which with continuity $ik\hat{u} + im\hat{w} = 0$ gives

$$\hat{u} = \frac{-\hat{p}}{\rho(U + iU_z/m)} \qquad (12)$$

In (12), if the background state is unsheared (independent of m), the perturbation velocity and pressure are in anti-phase as expected from Bernoulli's equation. Low pressure implies fast flow. If the shear dominates (with $U_z > 0$), the velocity will be delayed by 90 degrees from the pressure (if m is real). According to Figure 9b, the scatter around 90 degrees is small, suggesting that the influence of shear is small..

6. CONSERVED VARIABLE PLOTS

If the atmosphere is finely layered with conserved quantities such as ozone or water vapor, and then disturbed by a gravity wave, a level flying aircraft will penetrate these layers repeatedly, in forward and reverse order, as exemplified in Figure 10. Kinematically, it is similar to the encounter of a vertically sawtoothing aircraft with flat-lying layers. An example of ozone layering distorted by waves is shown in the conserved variable plot in Figure 11a. Theta is used as the vertical coordinate as it increases monotonically upwards. The range of theta is limited by the displacement amplitude of the wave (~500m). Note that the data curve traces and retraces the ozone profile as the aircraft flies through the wave.

A similar analysis can be applied to the dynamical layering in the flow, such as a fine scale upstream wind speed layering $U(z)$. To analyze these layers in the wave-disturbed region we use Bernoulli's Law. In steady perfect compressible flow the "mechanical" Bernoulli function

$$B = P(p) + (1/2)U^2 + gZ \qquad (13)$$

with

$$P(p) = \int v dp = \int \frac{dp}{\rho} = Kp^{1-1/\gamma} \qquad (14)$$

and $K = p_0/\rho_0(1-1/\gamma)$ is conserved following a streamline (Prandtl,1934, Schaer, 1993). The incompressible version of (14) could also be used ($P(p) \approx p_0/\rho_0(1-1/\gamma) + p'/\rho_0$). Note that we do not use the so-called dry static energy (Gill, 1982) as a Bernoulli function, as it is dominated by the internal energy, and thus is partly redundant with theta. As with energy flux (7, 9), (13) cannot be evaluated without GPS altitude for the last term. In Figure 11b we show an example of Bernoulli layering. The tight (inverse) correspondence to the ozone layering suggests that the chemical and dynamical layering might arise from an interleaving of distinct air masses in the stratosphere, upstream of the Sierra region.

An independent observation of ozone and wind speed layering can be accomplished using aircraft soundings in cases with weak or no waves. These soundings confirm that the stratosphere is dynamically and chemically layered on scales of 100m. With waves, this speed layering contributes to the u' perturbations (Fig. 9b) and gives a false background to the horizontal kinetic energy (Section 3).

7. CONCLUSIONS AND FUTURE WORK

Using a statistical approach, we have attempted to describe Sierra mountain waves entering the stratosphere. Our data comes from the new Gulfstream V during the T-Rex project, and included GPS altitude measurements. The GPS altitude measurements were used in three computations: energy flux, phase relationship between p and u, and the Bernoulli function.

A striking aspect of the data is the variability from flight to flight and within flights. Our goal is to summarize wave attributes in a way that will challenge modelers and theoreticians, deepening our understanding of mountain waves. We hope to extend previous work on stratospheric waves by Lilly and others (1973, 1974, 1982).

An interesting but complicating factor is the pre-existing chemical and dynamical layering in the stratosphere (see also Salathe and Smith, 1992). While the layering adds to the background kinetic

energy and modifies certain phase relationships, it does not disturb the classical relationship between the energy and momentum fluxes.

Two aspects of the data remain unexplained. First, we found a local violation of equipartition in the upper troposphere. This would not be consistent with a simple vertically propagating wave, but it does not violate basic principles with regard to trapped or leaky lee waves.

The second curiosity was found in flight 10, where the energy and momentum fluxes changed sign at about 12km. Unlike flights 4 and 5 with positive EF at all levels, Flight 10 had negative EF above 12km. As the environmental conditions were similar to the other flights and no critical level was present below 21km, this energy flux convergence is unexplained.

In future work we will redo this analysis using calibrated aircraft data and compare these observations with data from balloons and the Wyoming King Air and with linear and full numerical models.

8. ACKNOWLEDGEMENTS

The assistance of T-Rex and NCAR staff during the field phase was essential. The ATC personnel in the Joshua Control Area were very helpful. The Yale group was supported by the National Science Foundation (ATM-112354 and -0531212).

9. REFERENCES

Eliassen A. and E. Palm, 1961: On the transfer of energy in stationary mountain waves. *Geofys. Publ.,* **22,** 2 1-23

Gill, A.E., 1982: *Atmosphere Ocean Dynamics*. Academic Press, 662pp.

Jiang, Q., et al., 2002: Mountain waves in the middle atmosphere: microwave limb sounder observations and analysis. *Advances in Space Research*, **C2**.1-0008-02, COSPAR-2002.

Lilly, D.K., Kennedy, P.J., 1973: Observations of a Stationary Mountain Wave and its Associated Momentum Flux and Energy Dissipation. *J. Atmos. Sci.*, **30**, 1135-1152

D.K. Lilly and Peter F. Lester. 1974: Waves and Turbulence in the Stratosphere. *J. Atmos. Sci.*, **31**, 3 800–812.

Lilly, D. K., D. E. Waco and S. I. Adelfang, 1974: Stratospheric Mixing Estimated from High-Altitude Turbulence Measurements**.** *J. App. Met.,* **13**, 4 488–493.

Lilly, D.K, J.M. Nicholls, R. M. Chervin, P. J. Kennedy, and J. B. Klemp, 1982: Aircraft measurements of wave momentum flux over the Colorado Rocky Mountains**.** *Quarterly Journal of the Royal Meteorological Society*, **108**, 457 625-642(18).

L. Prandtl and O.G. Tietjens, 1934: *Fundamentals of Hydro- & Aeromechanics*. Dover, 270pp.

Salathé, E. and R. B. Smith, 1992: In Situ observations of temperature microstructure above and below the tropopause. *J. Atmos. Sci.*, **49**, 2032-2036.

Schaer, C., 1993: A generalization of Bernoulli's Theorem. *J. Atmos. Sci.*, **50**, 1437-1443.

RF	IOP	Date	Track	Mtn Top Wind (m/s)	W Max (m/s)	W Min (m/s)	Theta Range Max (C)	Theta Range Min (C)	KE Z kJ/m^2	KE H kJ/m^2	PE kJ/m^2	Domin. Wave Length (km)
01	1	M2	B	12.5								
02	2	M5	C									
03	3	M9	A									
04*	4	M14	B	16.3	11	3	19	3	40	700	600	40
05*	6	M25	B	24.2	14	2	25	1	50	700	500	17
06*	9	A2	B	13.1	3	1	14	1	4	80	20	15
07	IC	A7	IC									
08*	10	A9	B	12.5	7	2	9	1	9	65	45	14
09*	13	A15	B	11.5	6	2	15	1	6	75	95	14,24
10*	13	A16	B	15	20	8	21	4	120	800	750	30 (**15)
11	14	A21	C									
12	15	A26	B									

Table 1: T-Rex GV flights and data for focus flights
(* focus flights; ** above 12km)

Figure 1. NCAR Gulfstream V Research Aircraft

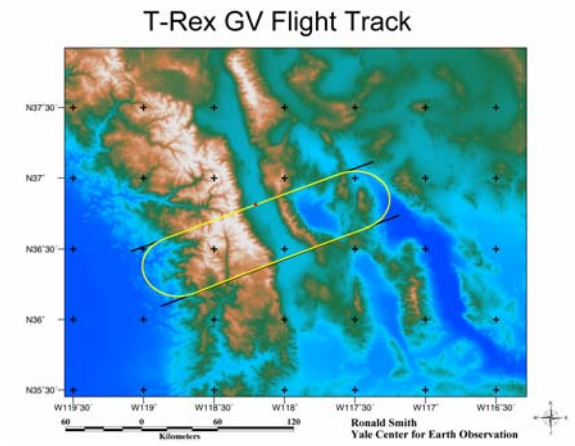

Figure 2. Racetrack over the Sierra Nevada Range

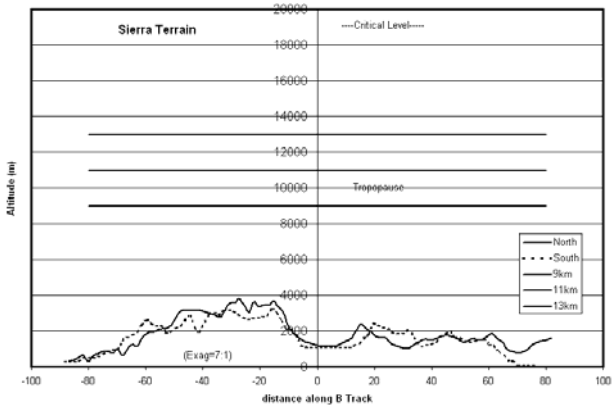

Figure 3. Vertical section over the Sierra showing the flight altitudes, tropopause and critical level

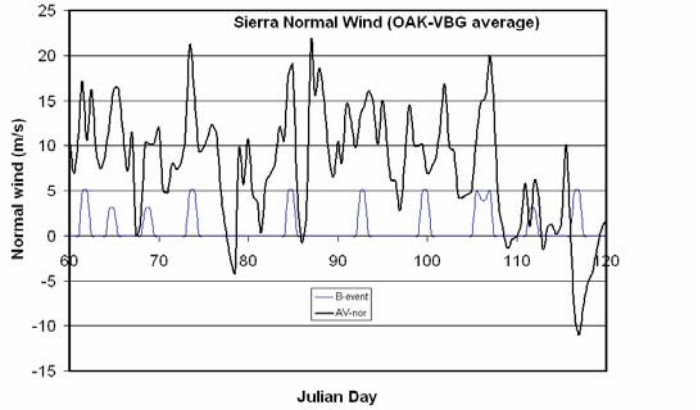

Figure 4. Cross mountain 700hPa wind from Oakland and Vandenburg soundings

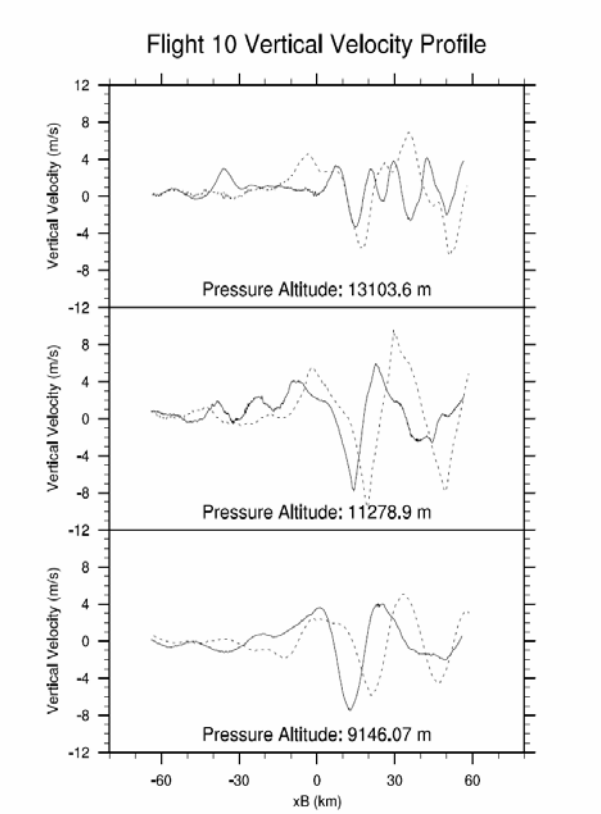

Figure 5. Flight level vertical air velocity from a stacked racetrack in flight 10 (north leg is dashed, south leg is solid)

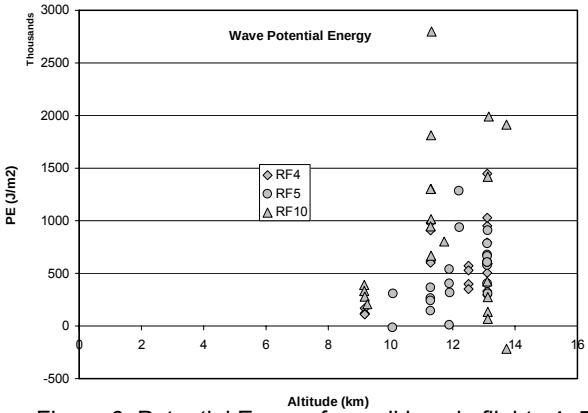

Figure 6. Potential Energy from all legs in flights 4, 5, 10

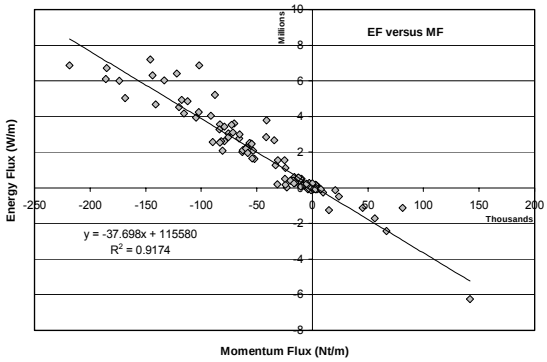

Figure 7. Momentum and Energy Fluxes in flights 4, 5, 10

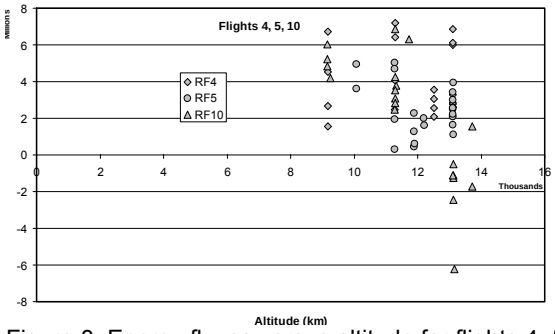

Figure 8. Energy fluxes versus altitude for flights 4, 5, 10

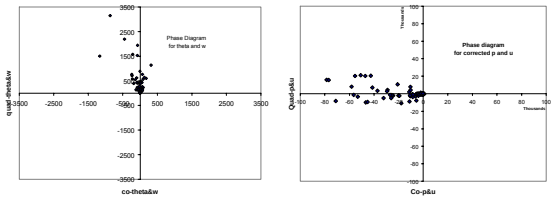

Figure 9. Phase diagrams for all legs: a) Theta and w, b) u and p

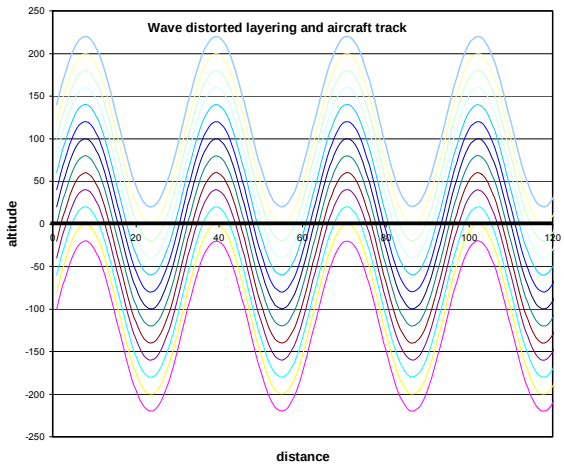

Figure 10. Schematic of atmospheric layers distorted by a wave. Aircraft path is horizontal.

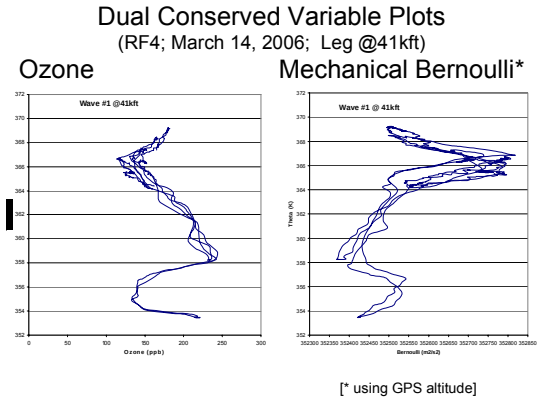

[* using GPS altitude]

Figure 11. Dual conserved variable diagram (ozone and Bernoulli function). Potential temperature is the vertical coordinate